Photopatterning of Dry Polymer Films: on the Relative Involvement of Diffusive and Capillary Convection in the Self-Corrugation Process

by **Daniel-Joseph Lougnot** and **Colette Turck**

Department of Photochemistry, UMR CNRS 7525 / APOLO, 3, rue A. Werner, F-68093 Mulhouse-Cédex

Dedicated to Professor *André M. Braun* on the occasion of his 60th birthday

Dry poly(vinyl alcohol) (PVA) formulations are widely used in the field of micro-optics for holographic recording and fabrication of micro-optical elements, but very little is known about the recording mechanism and even less in systems generating relief elements through a self-developing process. Thus, the recording of relief gratings with pitches ranging from 5 to 120 l/mm was examined with reference to the average weight of PVA and degree of hydrolysis. The slit width to pitch ratio in the amplitude mask used for photopatterning appeared to be also a controlling factor in the response of sensitive materials. A semiquantitative model was introduced to account for the final shape of the photogenerated relief. It determined the respective parts played by diffusion and capillary convection, *i.e.*, convection processes resulting from gradients of chemical potential and surface tension, respectively, and identified the experimental key parameters governing their interrelation. This work sheds new light on the optimization of the patterning conditions of amplitude masks and is expected to open up new vistas in the replication of computer-generated holograms.

1. Introduction. – For a few decades, polymer materials have been used in various fields of optical sciences as substitutes for traditional materials such as glass or fused silica. The specific features that motivate an extensive development are their simplicity of use together with very attractive optical properties and comparatively low cost. In this context, photopolymers have gained much interest on account of their ability to discriminate between various levels of light activation [1]. In fact, the degree of conversion of monomers to polymer depends on the fluence or dose of actinic light received by each part of the photosensitive formulation. Since this parameter goes hand in hand with the local value of the refractive index, swelling ratio, and solubility of the material and the surface tension of its upper interface, a replica of the spatial distribution of incident light can be stored in the photopolymer material. Quite interestingly, several groups have turned this unique property to advantage to generate binary or multilevel phase elements either with thickness or refractive-index modulation [2].

In the case of UV or electron-beam photolithography, each pixel of the polymer material undergoes more or less photoconversion depending on the dose of imaging light absorbed, hence the possibility of removing the non-crosslinked or depolymerized areas by solvent etching and storing the information as binary or multilevel relief elements. Clearly, this replication process is mainly limited by diffraction [3].

Besides this process, which requires a wet development or direct deep-UV etching with excimer lasers, a new procedure was recently introduced for the carving of photosensitive materials or the generation of relief thereupon. It is based on the self-

corrugation of the surface of photo-cross-linkable polymer films that results from the combined effects of a gradient of photonic activation with the gradient of surface free energy resulting therefrom [4]. This corrugation was believed to result from a flowing of the formulation, during or immediately after the conversion process, from dark to bright areas of the imagewise incident beam of actinic light. The driving force of this process would be the consequence of the gradient of monomer conversion which goes along with a gradient of chemical composition and chemical potential. To minimize the consequences of the corresponding gradient of surface tension, an increase in the area of the elements where surface tension decreases because of monomer conversion would take place. Interesting results were reported with systems based on this idea. In particular, low-frequency gratings (<200 l/mm) and microlens arrays ($50 < \phi < 500$ μm) exhibiting high optical quality have been generated in acrylate resins both by mask projection or imaging [5]. In spite of its very attractive features, the major drawback of this kind of material is its sticky surface that does not lend itself to contact printing. Thus, a gap is required between the amplitude mask and the resin, and, hence, this is an unavoidable limitation of the photonic transfer function due to light spreading. Another inconvenience results from fast self-development of the relief, which may start during the illumination, thus causing a distortion of the light field in the core of the film that degrades the response of the material.

The present paper deals with a dry photosensitive formulation, the corrugation of which self-develops mainly after imagewise illumination is completed. This formulation contained poly(vinyl alcohol) as a binder and a vinylpyrrolidinone/bis[acrylamide] blend that causes the linear binder structure to cross-link, thus generating a 3D-polymer network.

2. Materials and Methods. – The reactive formulation used was obtained from an aq. soln. of linear poly(vinyl alcohol) (60 g/dm^3 PVA) in which 15 g/dm^3 of vinylpyrrolidinone (=1-ethenylpyrrolidin-2-one; VP) and 3 g/dm^3 of methylenebis[acrylamide] (=*N*,*N*′-methylenebis[prop-2-enamide]; MBAA) were dissolved. The initiating system was eosin Y (optical density of the dry film @ 532 nm = 0.25) together with methyldiethanolamine (=2,2′-(methylimino)bis[ethanol]; MDEA; 80 g/dm^3).

From a photochemical viewpoint, the initiation process involves photoreduction of eosin triplet state by MDEA and subsequent attack of monomer molecules by the aminyl radical resulting therefrom [6]. A crosslinked VP/MBAA copolymer is thus generated. Because of the presence of tertiary H-atoms on the PVA chain, a transfer mechanism between the growing macroradicals and the binder may take place; this process creates macroradicals on the PVA main chain, which are annihilated by reaction with any radical present in the system. Links between the PVA continuous phase and the VP/MBAA photocopolymer clusters are thus produced; they favor compatibility and ensure excellent optical transparency. The possibility of a reaction between semireduced eosin and PVA macroradicals cannot be ruled out. Due to the small size of this species compared to VP/MBAA macroradicals, the consequences of this reaction can be disregarded.

$\text{Eosin}^* + \text{MDEA} \rightarrow \text{Eosin}^{\cdot -} + \text{MDEA}^{\cdot +}$	Oxydo-reduction
$\text{MDEA}^{\cdot +} \rightarrow \text{MDEA}^{\cdot} + \text{H}^+$	Acid-base equilibrium
$\text{MDEA}^{\cdot} + \text{Monomer(s)} \rightarrow \text{Macroradical}^{\cdot}$	Initiation
$\text{Macroradical}^{\cdot} + \text{PVA} \rightarrow \text{Poly(VP/MBAA)} + \text{PVA}^{\cdot}$	Transfer
$\text{PVA}^{\cdot} + \text{PVA}^{\cdot} \rightarrow \text{3D-PVA}$	Radical annihilation
$\text{PVA}^{\cdot} + \text{Macroradical}^{\cdot} \rightarrow \text{Grafted-PVA}$	Radical annihilation
$\text{Macroradical}^{\cdot} + \text{Grafted-PVA} \rightarrow \text{3D-Macroradical}^{\cdot}$	Transfer

A small amount of this liquid formulation (2.3 ml) was deposited onto a *Pyrex* glass slide (28 × 76 mm) and allowed to evaporate at r.t. on a perfectly horizontal plane in a box containing a moisture trap. After two days, the samples were ready for use or could be stored under the same conditions without substantial alteration of their appearance or photosensitivity. This drying procedure, which involved control of the ambient humidity by

a saturated NH_4NO_3 soln. (55% humidity) ensured perfect reproducibility of the photosensitivity of the samples throughout long storage periods or series prepared from successive batches. Under these experimental conditions, the average thickness of the samples was 85 ± 5 μm, and their H_2O content stabilized to ca 30%.

Two different light sources were used to photopattern dry PVA films. The former was a high-power illuminator (*Oriel* solar simulator) equipped with a *HBO-350-W* mercury arc and a beam homogenizer. The available light-power density in the actinic range of the sensitizer dye was ca 255 mW/cm^2; it is referred to as the 'high-power source'. Unless otherwise stated, this source was used to photopattern the samples throughout the experiments described in this report. The latter was a *HBO-100-W* mercury arc, which, after spectral filtering and collimation, delivered *ca.* 19.5 mW/cm^2 in the 546.1 line; it is referred to as the 'low-power source'.

After patterning through an amplitude mask in close contact with the polymer surface, the samples were left for 3 min in the dark, then illuminated for 1 min with the high-power source so as to ensure complete conversion of unreacted ethylene bonds and cancel any residual photosensitivity. After this treatment, the sensitizer dye was bleached, and the sample exhibited a fairly good surface flatness. To favor the dissipation of unrelaxed strain and allow evaporation of free molecules, the samples were stored for a few days at 45° in the dark. The records were stable for months, and the sensitivity of cross-linked material to humidity was very low. The *Persoz* hardness was measured to be 250 ± 30 s, which is equivalent to values currently measured for urethane acrylate polymers [7].

The topographic analysis of the samples was carried out with either a laser profilometer (*UBM Messtechnik*) or an atomic-force microscope (*Molecular Imaging*) in tapping mode.

3. Experimental results. – 3.1 *Step Grating Patterning*. Motivated in part by the desire to understand more about the system in which self-corrugation occurs, we carried out a lengthy detailed and systematic investigation of the frequency response of this new material. With this end in view, a set of 24 gratings (10×1 mm) with frequency increases in steps of 5 l/mm from 5 to 120 l/mm was generated according to the reference patterning procedure described in *Sect. 2*. This experiment was carried out on a sample of PVA with M_r 14000 and hydrolized to 100%. Preliminary experiments showed that the patterning of the photoactive surface produced a positive image, *i.e.*, with grooves corresponding to the dark regions of the amplitude mask.

General Behavior. The maximum height of the corrugation (h) plotted against the grating frequency (*Fig. 1*), showed a dramatic decrease from *ca.* 8 μm down to 150 nm from one end of the chart (5 l/mm) to the other (120 l/mm).

The corresponding experimental results can be displayed in another way by introducing a dimensionless parameter – the modulation ratio – that is defined in *Eqn. 1*. By plotting ρ against the grating frequency, an interesting curve was obtained (*Fig. 2*). An increase in ρ is observed between 5 and *ca.* 40 l/mm; then, it goes through a maximum and decreases monotonically. Without going into the details of physico-chemical aspects of the recording process, this feature would suggest, at least qualitatively, that it cannot be regarded as a single process proceeding identically over the range of spatial frequencies studied. It should rather be considered the result of a convolution between two elementary processes affected in opposite directions by an increase of the grating frequency.

$$\rho = \frac{\text{max. amplitude of modulation}}{\text{grating period}} \tag{1}$$

Another interesting feature was revealed by analysis of the frequency dependence of the shape of the fillets (the prominent parts of relief gratings). The characteristic parameter used in this case was the normalized width at half-maximum (*NWHM*). It

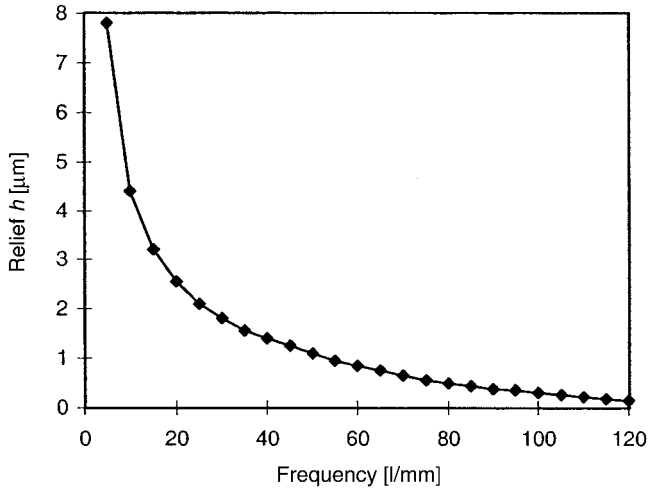

Fig. 1. *Maximum amplitude of the thickness modulation in the reference system*

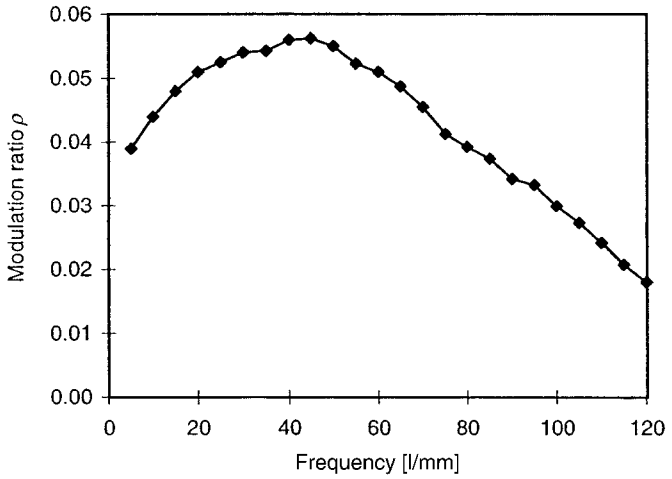

Fig. 2. *Modulation ratio ρ in the reference system*

was defined by *Eqn. 2*. *Fig. 3* shows the experimental results measured along the grating chart. They have to be compared to 0.5, a value that would denote a linear response of the material. Quite interestingly, the curve levels off at $NWHM \approx 0.67$ in the low-frequency range ($5 < \nu < 15$ l/mm), then decreases dramatically and levels off again near 0.46 in the higher-frequency range ($45 < \nu < 120$ l/mm). Such a behavior, which denotes a high degree of nonlinearity supports the same conclusion as before, *i.e.*, two controlling factors prevailing, the former one at low frequency and the latter at higher frequency.

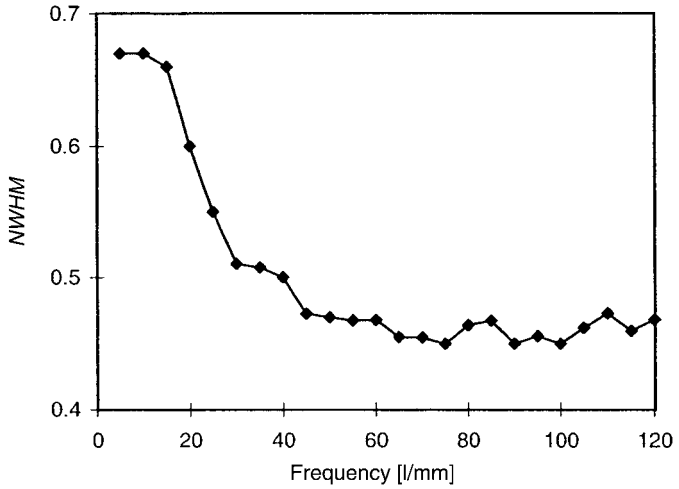

Fig. 3. *Normalized width at half-maximum* (*NWHM*) *of the positive corrugation in the reference system*

$$NWHM = \frac{\text{width at half-maximum}}{\text{grating period}} \tag{2}$$

With a view to better identify and understand the key factors accounting for the shape of the corrugation obtained by the reference patterning procedure, another parameter was used to characterize the gratings. The length of the profile along the axis corresponding to the grating's wave vector, *i.e.* the length of a trace drawn on the grating surface perpendicular to the grooves, was compared to the grating period so as to define a lengthening ratio (ΔL) by *Eqn. 3*. Experimental values are reported in *Fig. 4* as a function of the grating frequency. In good agreement with the comments made on *Figs. 2* and *3*, it can be concluded therefrom that the relative lengthening of the grating profile increases and then decreases with increasing frequency. Again, the curve passes through its maximum in the range 20–25 l/mm.

$$\Delta L = \frac{\text{length of the experimental profile}}{\text{grating period}} - 1 \tag{3}$$

Influence of Monomer Chain Length. Since the self-generation of the relief by this patterning process involves transport of material by either convective or diffusive flow or both, these transfer processes are controlled by viscosity constraints and diffusivity, respectively. It is thus to be expected that changing the rheological parameters of the polymer binder would affect, to some extent, the recording characteristics of the sensitive formulation. To check the validity of this assumption, a sample with longer chains (M_r 89000) and the same hydrolysis ratio was substituted for the reference PVA (M_r 14000 and 100%-hydrolysed). The curves showing h, ρ, *NWHM* and ΔL are reported in *Fig. 5*, *a*–*d*. Basically, the general behaviour of this system remains unchanged with respect to the reference formulation. However, it is revealing fact that

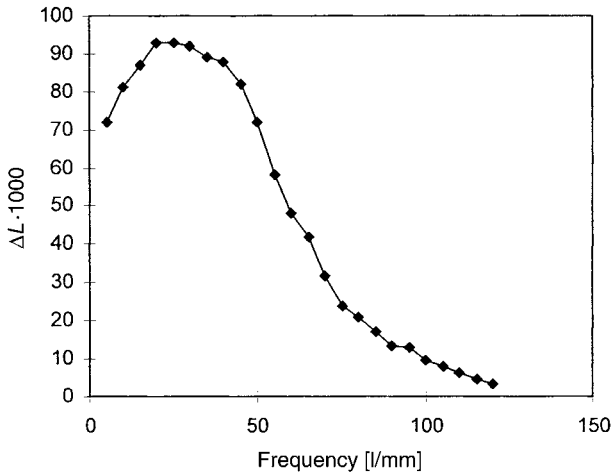

Fig. 4. *Lengthening ratio ΔL in the reference system*

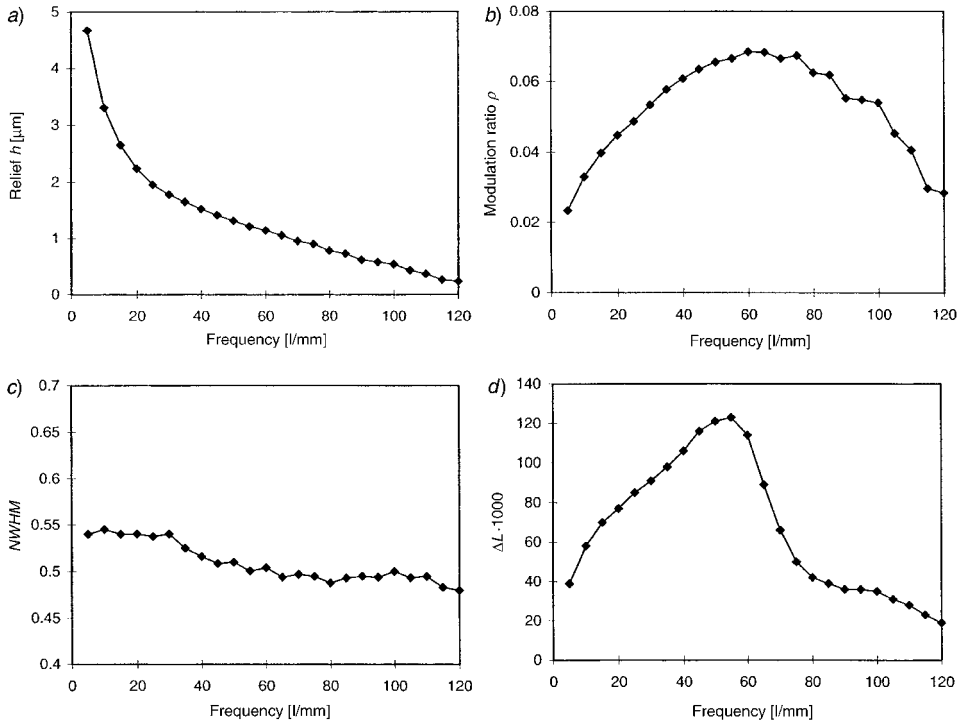

Fig. 5. *Characteristics of the gratings recorded in PVA of* M_r 89000 *and 100%-hydrolysed under intensity.* a) *Thickness modulation,* b) *modulation ratio* ρ, c) *normalized width at half-maximum* (*NWHM*), *and* d) *lengthening ratio* ΔL.

the curve of *Fig. 5, b*, exhibits its maximum at higher frequency, in the region of 65 instead of 45 l/mm. The same applies to the curve of *Fig. 5, d*, which passes through its maximum at 55 instead of 25–30 l/mm.

The thickening of the recording material that goes along with polymer-mass increase might account for these observations: the balance between capillary and viscosity constraints slows long-distance transport so that the medium part of the corrugations cannot grow to complete fill. Thus, this formulation is less suited for the generation of low-frequency gratings.

Influence of the Initiating Rate. The initiating rate (R_i) determines the polymerization rate and the time dependence of the conversion degree of monomer moieties to the corresponding polymer. It is thus a key parameter that controls the contrast of surface tension between bright and dark areas generated by image-wise irradiation and the amplitude of the capillary constraint resulting therefrom.

Although R_i is proportional to the light intensity absorbed by the photo-cross-linkable formulation, the overall analysis of the kinetics of conversion must not be restricted to this factor. Among other things, it depends greatly on the quenching process resulting from the presence of dissolved O_2, the inhibiting effect of which grows more detrimental as irradiance becomes weaker. Consequently, this quenching also affects the profile of the conversion ratio along the z axis (normal to the grating surface): while it is almost constant over the whole thickness of the layer under higher irradiances (*i.e.* when the effects of O_2 quenching can be disregarded), it remains very low near the surface, then it increases, and levels off in the bulk in systems photoconverted under lower irradiance. This gradient along the z-axis may introduce further complexity into the analysis of the hydrodynamics of relief development [4].

It is thus evident from the foregoing that the changing light-power density or spectral distribution of the actinic light makes it difficult to calculate the appropriate exposure that would achieve a constant overall conversion degree of the material. Since a trial-and-error approach alone was possible, it was observed that a 15-min exposure of the reference formulation to the 546-nm line of the *HBO* source was almost equivalent to a 15-s exposure to the high-power illuminator in terms of amplitude modulation.

Fig. 6, a–d, shows the frequency dependence of the parameters used to characterize the set of gratings obtained under low-power illumination. Although their general features resemble those of systems described before, two distinctive trends should be emphasized: no relief emerges from the background noise beyond 80 l/mm, and the modulation and lengthening ratio go through their maxima at very low frequencies (*ca.* 15 l/mm) compared to the reference system.

Due to O_2 quenching, the decrease in surface viscosity that goes along with lower conversion near the surface favors convection transport, thus making the growth of low-frequency corrugations easier. Likewise, the influence of diffusive transport becomes predominant at higher frequencies, so that the gradient of surface tension eventually vanishes due to fast equalization of the surface tensions in the adjacent bright and dark areas, hence the impossibility to photopattern in this range of frequency under mild photonic conditions.

3.2. *Gratings with Variable Cycle Ratios.* The lessons drawn from the experiments reported above substantiated the parts played by convective and diffusive transport phenomena and emphasized their interdependence. Changing the cycle ratio of the

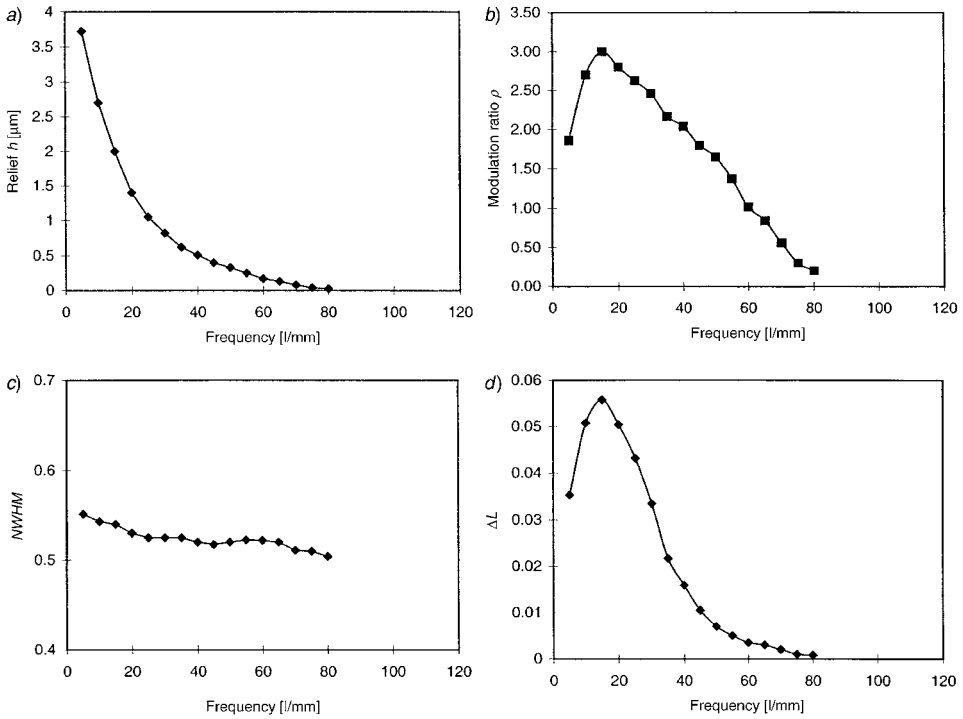

Fig. 6. *Characteristics of the gratings recorded in the reference system under low intensity.* a) *thickness modulation,* b) *modulation ratio* ρ, c) *normalized width at half-maximum* (*NWHM*) *and* d) *lengthening ratio* ΔL.

incident amplitude pattern appears a clever means allowing to shift the balance between capillary and viscous constraints and to change the relative contributions of convective and diffusive flows to the growth of the relief. This ratio is defined by *Eqn. 4*.

$$r = \frac{\text{slit width}}{\text{opaque strip width}} = \frac{\text{slit width}}{\text{grating period} - \text{slit width}} \tag{4}$$

A chromium mask (1000 l/inch $\approx$ 40 l/mm, *i.e.*, grating period = 25.4 µm) whose characteristics are described in the *Table* was used for this purpose. The increase of the cycle ratio is softer in the range covering lower ratios where the behaviour of the system seems to be more dependent on the slit width.

General Observations. Fig. 7 reports the response of the reference formulation photopatterned through illumination with both light sources described before (low and high intensities). The results obtained with the high-intensity source are quite consistent with what was intuitively expected, at least from a qualitative viewpoint. The height of the relief goes through its maximum for a cycle ratio close to unity (*i.e.*, corresponding to a symmetric binary amplitude mask), and either a decrease or an increase of this ratio induces a degradation of the patterning. Such a limitation is in agreement with those previously identified: narrowing the dark fringe decreases the

Table. *Characteristics of the Chart with Variable Cycle Ratio.* Grating frequency 1000 l/inch.

Number of the grating	Slit width [μm]	Cycle ratio
1	4.3	0.20
2	5.3	0.27
3	6.4	0.33
4	7.9	0.45
5	9.1	0.56
6	11.2	0.79
7	13.5	1.13
8	16.3	1.78
9	19.6	3.35

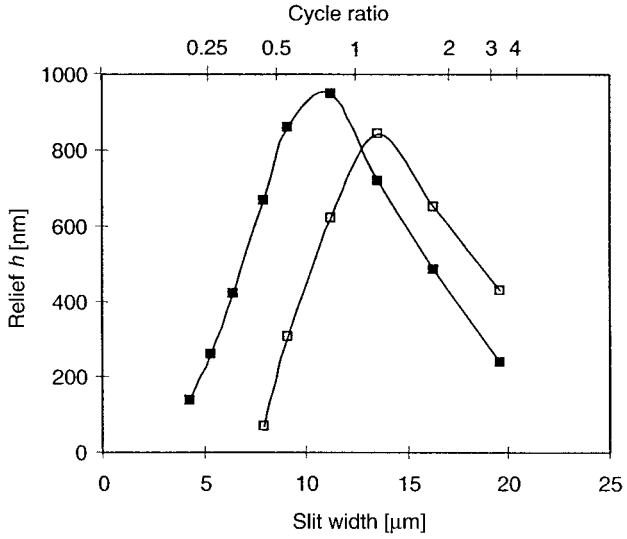

Fig. 7. *Amplitude of the relief recorded with variable cycle ratios: high intensity* (■) *and low intensity* (□). The recording system is PVA of M_r 14000 and 80%-hydrolyzed.

amount of material available for feeding the capillary-convection process; likewise, increasing its width lengthens the path between the reservoir and the center of the bright fringe where it is supposed to accumulate.

The general trends observed under weaker intensity are basically the same with a maximum corrugation amplitude shifted to higher cycle ratios (*ca.* 1.2 instead of 0.8). Another distinctive feature is a significant reduction of the height of modulation. In good agreement with the remarks regarding the influence of photonic parameters on the patterning process of symmetric binary-amplitude masks developed previously, attenuating the light-power density leads to a softening of the contrast and a smoothing of the relief profile. The shift of the maximum under low-intensity conditions with respect to that under high-intensity conditions (see *Fig. 7*) can be accounted for by an acceleration of diffusive convection due to a less-pronounced viscosity increase near the surface during the recording process. *Fig. 8* shows the dependence of *NWHM* as a

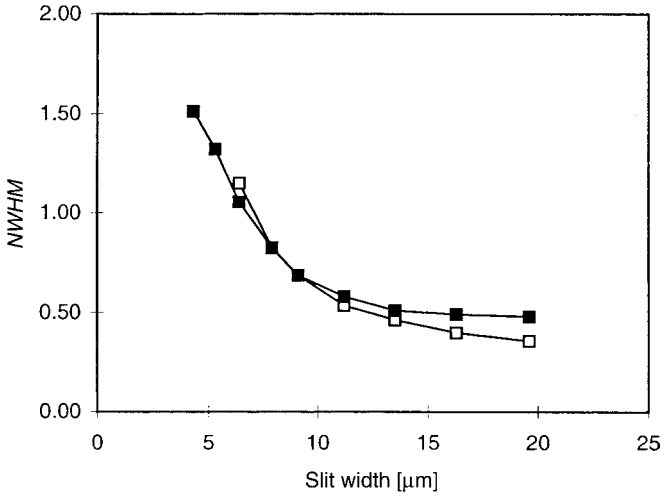

Fig. 8. *Normalized width at half-maximum* (*NWHM*): *high intensity* (■) *and low intensity* (□). Recording system as in *Fig. 7.*

function of the slit width for both high- and low-power densities. It reveals an interesting feature of the patterning process. Under intense illumination (and short exposure), the *NWHM* decreases steeply while the slit opens from *ca.* 4 up to 11 μm and then levels off close to 0.5 for slit widths exceeding 12 μm. This behaviour should prove suitable for applications requiring good linearity of the amplitude to phase-conversion process, *e.g.*, the replication of pixelized computer-generated holograms. Under weaker illumination conditions, the overall shape of the curve remained the same with a much less pronounced decrease at low slit apertures and levels down to *ca.* 0.37 for maximum cycle ratios. Clearly, these patterning conditions favor diffusive at the cost of capillary convection; the driving forces responsible for the corrugation of the polymer surface are smoothed, hence an important distortion of the transfer process occurs to make these operating conditions inappropriate for amplitude-to-phase replication of pixelized information in this range of frequency.

Influence of Plasticizers. Since the kinetics of capillary convection is greatly affected by viscosity constraints in a visco-plastic medium, complete relaxation of the surface and internal strain should be favored by a decrease in dynamic viscosity. To corroborate this statement, small amounts of low-molecular-mass poly(ethylene glycol) were incorporated into a formulation (15% *w*/*w* of PEG M_r 900) that was evaluated under the same experimental conditions as those of *Fig. 8*. While almost no significant change was visible under weaker illumination-power density, the steepest part of the *NWHM vs.* slit width curve was shifted to narrower apertures. With regard to this parameter, the range of fair linearity covers an extended range of cycle ratios from *ca.* 0.5 up to 3.3 (*Fig. 9*).

Influence of the Polymer Molecular Mass and Hydrolysis Ratio. Most of the studies concerned with PVA as either a binder medium or a reactive substrate for optical applications have left the macromolecular characteristics of the polymer chain out of

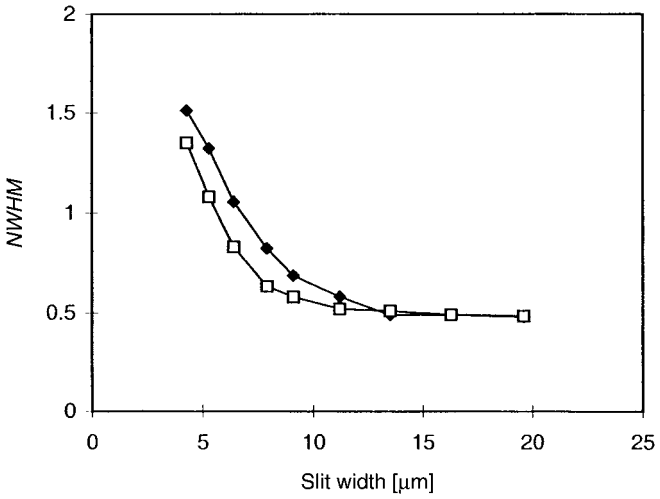

Fig. 9. *Normalized width at half-maximum* (*NWHM*): *without PEG* (■) *and with PEG* (□). Recording system as in *Fig. 7.*

consideration. However, in any investigation dealing with the macroscopic behaviour of this material, the properties strongly affected by its average molecular mass (*i.e.*, the chain length) and its hydrolysis ratio must be considered with special attention. It is well-known fact that PVA is not a native polymer; it is obtained by hydrolysis of poly(vinyl acetate), a reaction difficult to carry out to complete conversion. Two consequences arise therefrom: carboxylic groups usually terminate both ends of the linear polymer chain [8], and a significant proportion of the vinyl acetate moieties may not be hydrolysed to vinyl alcohol. Whenever any elementary step of a recording mechanism is pH-dependent, a marked influence of chain length on the patterning process can be observed. As to the degree of hydrolysis, the presence of poly(vinyl acetate) sequences can be suspected of introducing some degree of organization of the polymer in nanodomains, *i.e.*, a PVA-rich bulk phase where viscous properties are mainly under the control of H-bonding, and poly(vinyl acetate)-rich pools where dipolar interactions are prevalent. Substituting short polymer chains for longer ones reduces the acidity introduced by terminal carboxylic groups and the plasticity of the medium, whereas switching to lower hydrolysis degrees may affect the structure of the material at the nanoscopic scale and modify the polarity distribution of sites where elementary processes take place.

With a view to substantiating this statement, *Fig. 10* summarizes results obtained with two PVAs (M_r 14000 and 100%-hydrolysed, and M_r 10000 and 80%-hydrolysed) under high-power illumination conditions which admittedly are the most favorable in terms of patterning linearity. The small difference in M_r between these polymers should not significantly affect acidity and rheological properties in the investigated media. Conversely, incomplete hydrolysis can be reasonably expected to impair the cohesion of the starting polymer due to the presence of poly(vinyl acetate) microdomains. This trend should be accentuated by their poor affinity for acrylamide monomers, compared

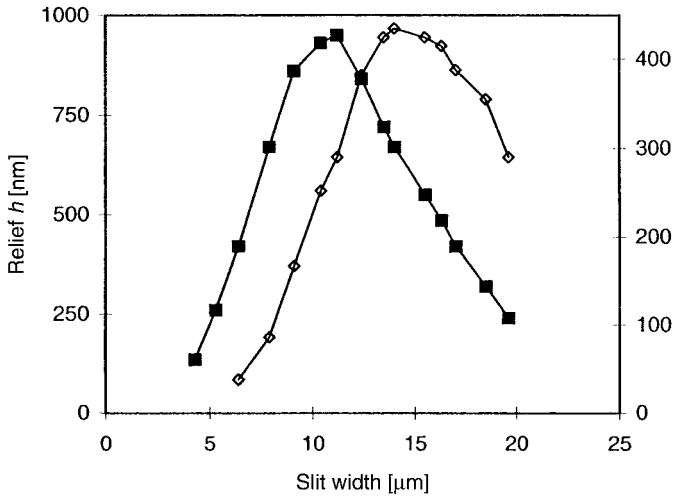

Fig. 10. *Influence of the hydrolysis ratio on the thickness modulation: 80%-hydrolysed PVA* (■) *and 100%-hydrolysed PVA* (□)

with homoPVA, which reduces their propensity of stiffening through photoinduced cross-linking.

The overall shapes of the curves reported in *Fig. 10* are very similar. They differ only by their amplitude at maximum and their position with respect to slit widths, *i.e.*, the maximum amplitude of modulation is obtained for broader slit apertures with 100%-hydrolyzed than with the 80%-hydrolyzed PVA. These observations are in line with the previous remarks: due to more pronounced stiffening, the former one requires a stronger driving force to reach the same degree of corrugation than the latter. Under the same patterning light power, only the use of a mask with broader slit widths can meet this requirement.

4. Modelling Capillary Convection in Dry PVA Films. – The behaviour of a liquid-liquid or a liquid-air interface is governed by surface tension that controls hydrodynamic flows involved in the convection movements of a fluid layer. Gradients of surface tension related to variations of a scalar parameter such as temperature or concentration induce surface strain and hence flows in the liquid. In the system under examination, γ, the surface tension (or interfacial tension), depends on the chemical composition of the underlying formulation, *i.e.*, the local value of the monomer-to-polymer conversion ratio.

Although exact experimental determination of γ is not yet possible, it is well-known fact that the conversion of ethylene double bonds to their corresponding aliphatic homologues (monomer to polymer conversion) goes along with a decrease of γ in the order of 15 to 25% [9].

4.1. *Some Key Ideas for Modelling.* Consider first the dependence of γ along the x coordinate (collinear with the grating's wave vector) (*Eqn. 5*). A concentration gradient parallel to the surface of the liquid phase, thus, induces a tangential stress

therein. The factor α accounts for the change of surface energy and surface tension as the monomer molecules generate a 3D-polymer network in the illuminated areas of the recording medium. In a first approximation, it can be assumed to be constant since the molar fraction of monomers dissolved in the PVA binder is low. Further, α is positive, which denotes a decrease in surface tension related to the conversion of ethylene unsaturations to aliphatic C–C bonds. The minus sign means that the driving force is oriented towards the region where surface tension decreases, *i.e.*, where conversion is maximum.

$$\frac{d\gamma}{dx} = \left(\frac{\partial\gamma}{\partial c}\right)\frac{dc}{dx} = -\alpha\frac{dc}{dx} \tag{5}$$

Thus, when the surface of the recording medium is submitted to a spatially controlled irradiation, a flow of reactive formulation takes place near the surface from the dark to the bright areas. Modeling this flow should take the following ideas into consideration [10]: *i*) In a first approximation, *i.e.*, disregarding volume shrinkage associated with monomer conversion, the overall volume of the recording material is a constant. *ii*) In the dynamic description of the recording process, the limit conditions correspond to the equality of the tangential capillary constraint and the viscous constraint Σ_{xz} according to *Eqn. 6*, where η is the dynamic viscosity, and u and w are the projection of the flow rate along the grating's wave vector and the normal to the initial surface, respectively. Because there is no flow along the slit direction, this index can be dropped.

$$\Sigma_{xz} = \eta\left(\frac{\partial u}{\partial x} + \frac{\partial w}{\partial z}\right) \tag{6}$$

iii) Since the visco-elastic material is a linear polymer in which cross-links are progressively created as photopatterning proceeds, the diffusivity of small molecules is time-dependent. Consequently, the momentum-flow balance swings more and more to capillary convection. The contribution of diffusive transport becomes insignificant, eventually.

In a system where the initial distribution of diffusing species occupies a finite region, their concentration is described by *Eqn. 7* [11], with $C(x) = C_0$ for $x < 0$ and $C(x) = 0$ for $x > 0$ at $t = 0$. In the case of a system irradiated through a line-mask, the concentration distribution corresponding to the initial state of diffusion is periodical along the grating's wave direction with alternate regions of high ($c_{o\,max}$) and low ($c_{o\,min}$) concentration and equal width (d). The concentration can then be written as in *Eqn. 8*.

$$C(x,t) = \frac{C_0}{2} erfc\frac{x}{2\sqrt{Dt}} \tag{7}$$

$$C(x,t) = C_{0\,min} + \frac{C_{0\,max} - C_{0\,min}}{2}\sum_I \left[erf\frac{(2i+1)d - x}{2\sqrt{Dt}} + erf\frac{(2i+1)d + x}{2\sqrt{Dt}}\right] \tag{8}$$

The distribution at successive times is shown in *Fig. 11* by means of normalized dimensionless coordinates: along the grating's wave direction by x/d, and as diffusion proceeds by k as defined in *Eqn. 9*. The ordinate corresponds to the ratio of the actual

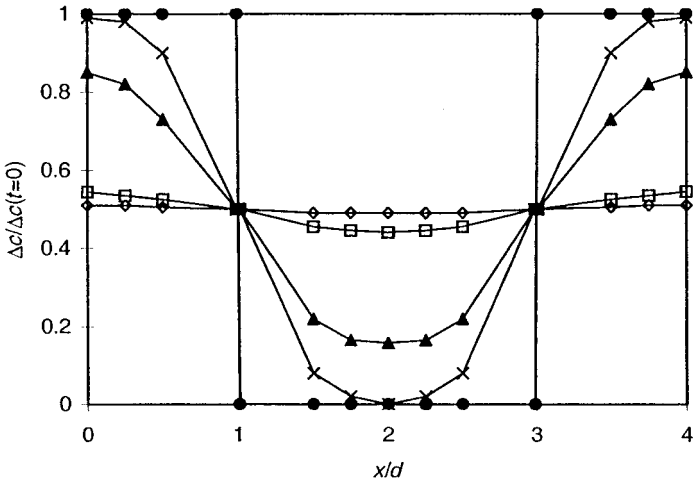

Fig. 11. *Diffusion profiles for various values of the dimensionless coordinate* k (○, 0; ×, 0.25; ▲, 0.5; □, 1; ○, 2)

concentration modulation – $(c_{max}(t) - c_{min}(t))$ – to the value of this modulation at time zero. This parameter is referred to as $\Delta c/\Delta c(t=0)$.

$$k = \frac{\sqrt{Dt}}{d} \tag{9}$$

Any quantitative analysis of the recording dynamics should be based on this description of the concentration dependence of diffusing species, which makes it possible to calculate the spatio-temporal value of the surface-tension gradient. Determining some of the experimental parameters (*e.g.* diffusivity) is difficult, so that only a semiquantitative approach is possible. Thus, the amplitude of the concentration modulation (Δc) can be derived from this spatio-temporal dependence of c as a function of the dimensionless parameter k defined before. It can be used as an indirect indicator of capillary-constraint intensity.

Clearly, the curve in *Fig. 12* reveals the existence of two contrasting regimes in the coupling of diffusion and convection. *a*) The condition $\sqrt{Dt} < 0.5d$ prevails whenever the recording time is short (*i.e.* under high recording power) and/or when recording materials are characterized by a low diffusivity of the mobile species. It corresponds to a recording process where transport is under the control of capillary convection.

b) The condition $\sqrt{Dt} > d$ prevails in softer formulations and/or when weaker actinic intensities are used to pattern the sensitive material. In this configuration, the photogenerated gradient of surface tension is smoothed by diffusive convection, and the relief resulting from capillary transport decreases, and, eventually, corrugating the material becomes impossible.

Interestingly, entering $d = 12$ μm (the slit-width in the medium part of the chart with variable cycle ratio) and $t = 15$ s (usual exposure with the high-power source) leads to a critical diffusivity (D corresponding to the turning value between the two regimes

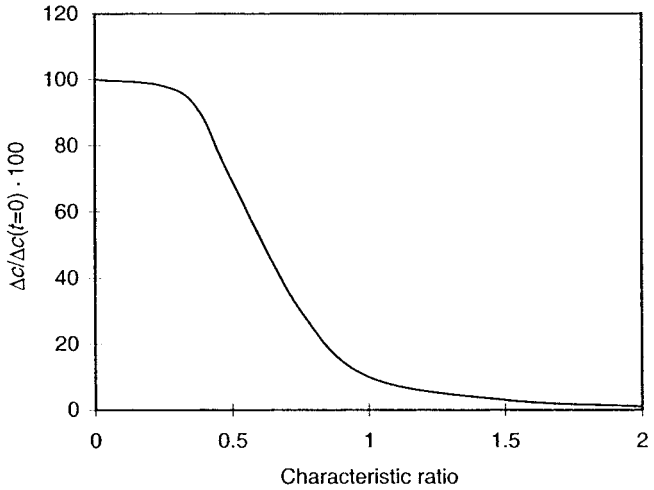

Fig. 12. *Ratio of* $C_{max} - C_{min}$ *to* $C_{0\,max} - C_{0\,min}$ vs. *the dimensionless coordinate* k

described above) in the order of 10^{-11} m^2/s. This value is in good agreement with values reported in the literature for dry soft-gel polymers [12].

4.2. *Shape of Grating Profile.* A time-dependent dynamic viscosity characterizes the recording system that is the seat of a photo-cross-linking process. It is, thus, hardly conceivable to elaborate an analytical description of the diffusion coefficient of mobile species in such a medium. At the very most, some general trends based on the semiquantitative approach developed above can be emphasized. In addition, the build up of thickness modulation driven by gradients of surface tension may stop before reaching a minimum of free energy because of polymer cross-linking which goes hand in hand with surface profile reshaping. Its gelation may cause the system to stiffen, thus preventing the surface from bending any further.

On the other hand, a static description of the profile based on the *Young-Laplace* law is possible. This law states that the curvature of the interface separating two semi-infinite media should obey *Eqn. 10*, where Δp is the difference of pressure between the two media, γ the interfacial tension, and R the curvature radius of the interface.

$$\Delta p = \frac{\gamma}{R} \tag{10}$$

In the system under examination, the photopatterning process triggers some irreversible chemical reactions that accompany corrugation of the recording material: these changes occur together with an increase in the energy of the system (ΔE). From a physical viewpoint, the dimensions of this variation and of Δp are the same (force by surface unit or energy by volume unit). On the right-hand side of *Eqn. 10*, both γ and R, whose values are not constant along the grating profile, can be expressed as functions of the spatial coordinates. On the basis of these facts, the differential form of the *Young-Laplace* law is written in *Eqn. 11*, and after integration over one period of the grating, *Eqn. 12* results.

$$dE = \frac{\gamma(x)}{R(x)}dx \tag{11}$$

$$\Delta E = \int_0^{2h} \frac{\gamma(x)}{R(x)}dx \tag{12}$$

In this expression, $\gamma(x)$ is directly related to the chemical composition of the underlying volume element, and ΔE accounts for entropic variations; the two factors, which are controlled by diffusion, were calculated. The analytical expression of $R(x)$ or at least its numerical value should, thus, be available. It must be kept in mind, however, that $\gamma(x)$ and ΔE are time-dependent because the photoprocess goes on along with relief self-development; hence it is the impossibile to know if the growth of a grating at a given time is under kinetic (hydrodynamic) or thermodynamic control.

4.3. *Types of Grating Shapes.* From the previous statement, it is evident that several behaviours can be observed depending on the set of characteristic parameters attached to each of the systems under examination. The simplistic approach used to categorize a few typical examples considers the grating frequency, shear modulus, and rate of curing as 'boolean' parameters, *i.e.*, with a low and a high value, only.

Low Shear Modulus and Fast Curing. The driving force that is responsible for surface grooving is counterbalanced by a low viscosity constraint. The system relaxes its strain through bending of the regions where the gradient of surface tension is maximum; the stress elements resulting from the concave curvature on both sides of the depleted regions are balanced by those associated with the convex edges of the protruding parts of the grating. Due to the low contribution of viscosity constraint, which allows long distance transport by convection, the central part of both bright and dark regions is flat; the widths of the transition regions where slight interdiffusion and diffraction affect the profile of the gradient are reduced to a minimum; then, the grating exhibits a binary profile. *Fig. 13*, *a*, exemplifies this class of profiles.

Low Grating Frequency and Fast Curing. In this case, viscous constraints do not allow the convective flow driven by capillary constraints to reach the medium part of the bright areas before the system undergoes gelation. It results, therefore, in a crater profile with a more or less pronounced dip in the middle (*Fig. 13*, *b*). In this case, upward and downward stress contributions balance each other through an increase of the curvature in the concave portions of the profile.

High Grating Frequency. The dominant factor that controls the shape of the profile is the response to the sharp changes in surface tension at the edges of the bright areas. Since the consequences of interdiffusion and diffraction by the edges of the slits are felt up to the center of bright and dark regions, no portion of the patterned surface can be found where surface tension is constant. Thus, the grating exhibits a bell-shaped profile (*Fig. 13*, *c*).

High Grating Frequency, Low Shear Modulus, and Slow Curing. This situation corresponds to the case of a material in which diffusive convection overwhelms capillary convection; the gradient of chemical potential generated by the patterning process is gradually cancelled by diffusion so that the gradient of surface tension remains too weak all along the profile to trigger capillary transport.

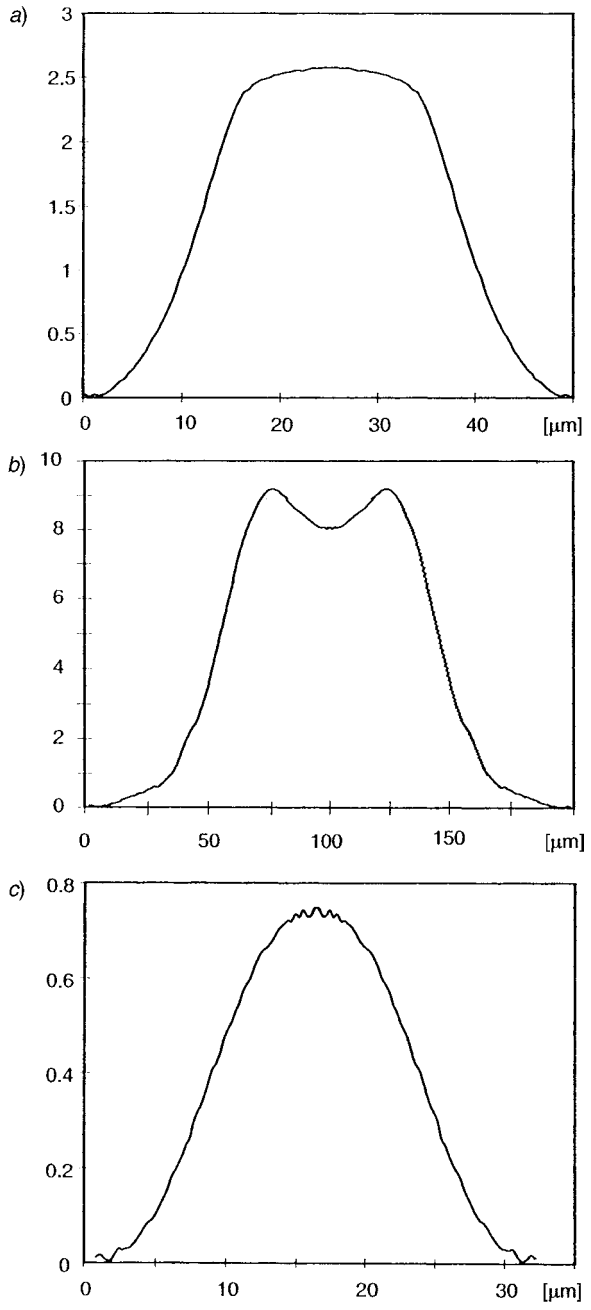

Fig. 13. *Various possible shapes of the relief:* a) *20 l/mm,* M_r *14000 and 100%-hydrolysed, high intensity,* b) *5 l/mm,* M_r *89000 and 99%-hydrolysed, low intensity, and* c) *30 l/mm,* M_r *14000 and 100%-hydrolysed, low intensity*

4.4. *Grating Shape and Development of the Profile.* Parameter ΔL was introduced to measure the lengthening of the profile along the chart with increasing grating frequency. It is worthwhile to compare ΔL shown in *Fig. 4* with the lengthening that would correspond to gratings with an ideal binary shape (ΔL_{bin}) and the same heights as those shown in *Fig. 1*. The same could also be done by assuming a purely sinusoidal shape (ΔL_{sin}). *Fig. 14* shows the results of these calculations. It is worth of notice that $\Delta L_{exper.}$ approximates closely ΔL_{bin} in the lower-frequency range, whereas it tends to fit ΔL_{sin} in the 100–120 l/mm range. This observation corroborates the previous statements and gives another experimental evidence for the degradation of the photochemical transfer function as frequency increases. The same was done with results of *Figs. 5,d*, and *6,d*, and the conclusions arrived at are nearly the same.

In the higher-frequency range, although the shape of the relief is very close to a sinusoidal profile, careful examination of results obtained under a great variety of experimental conditions suggests, however, that they are better fitted to the analytical function of *Eqn. 13* (*Fig. 15*). With respect to x, this function is the derivative of *Eqn. 8*, within a constant, *i.e.*, it is proportional to the gradient of concentration resulting from square-spatial-wave modulation of the photochemical activation and subsequent smoothing through diffusion. It results therefrom that the amplitude of the relief would be proportional to the capillary constraint whose relaxation becomes predominant after transport by diffusion runs out, due to complete conversion of the reactive species. This provocative conclusion calls for further substantiation.

$$h = \sum_{i}^{-\infty;+\infty} \exp\left(-\frac{(x + 4i\sigma)^2}{\sigma^2}\right) \tag{13}$$

5. Conclusions. – An interesting self-processing formulation for photopatterning was developed. Because of the dramatic change of rheological properties between the

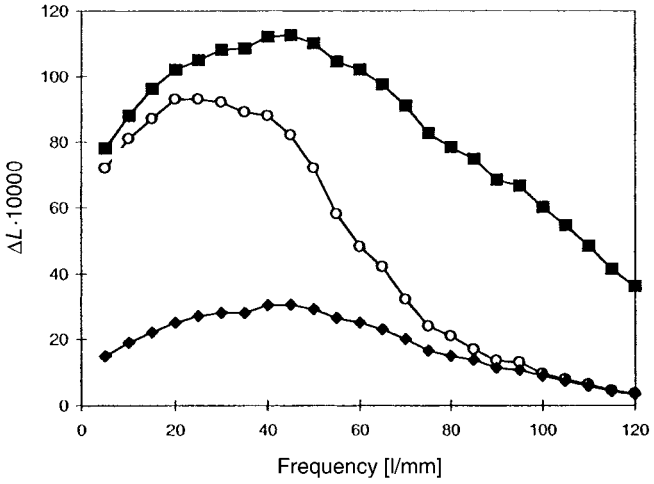

Fig. 14. *Experimental lengthening ratio* vs. *calculated lengthening ratios: binary profiles* (■), *sinusoidal profiles* (◆) *and experimental profiles* (○)

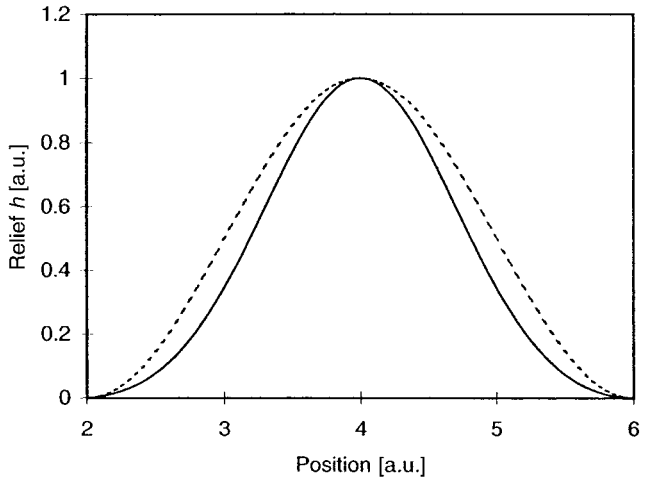

Fig. 15. *Profile calculated from* Eqn. 13 *with* $\sigma = 1$ (–) *compared to a sinusoidal profile with the same amplitude modulation and period* (- - -)

beginning of the recording process and the final stage of its stabilization, diffusion and convection transport were turned to the best possible account. Due to a cross-linked structure and thermal post fixing, this formulation exhibits outstanding mechanical stability. In addition, its tack-free surface makes it a perfectly suited candidate for contact printing or proximity printing as well. In short, its recording properties outstrip by far those of PVA [13].

In a preliminary, semiquantitative approach to modelling the profile of the relief photogenerated in this type of formulation, the key parameters governing the recording process and the optical properties of polymer elements were identified. The driving forces responsible for the self-corrugation of the photopatterned surfaces are capillary convection and *Fick*'s diffusion. The former is triggered by the gradient of surface free energy associated with space-controlled double-bond conversion. It induced flow of the liquid formulation at the surface layer, without change of chemical composition. The latter takes place near the edges of the areas activated by a spatial square wave, *i.e.*, where the gradient of chemical potential is higher. It induces transport phenomena on the molecular scale, which result in a smoothing of the discontinuities of chemical composition. These driving forces are balanced by viscosity constraints. Due to the complex gel character of the recording media, self-development of the photogenerated corrugation is not instantaneous; it starts during photopatterning and homogeneous post-illumination and then proceeds up to completion in the dark.

Promising results that found experimental support were obtained. In spite of its unfinished character, this study can be expected to open up new vistas in the field of refractive micro-optics or hologram duplication.

The authors are indebted to Dr. *H. Haidara* for valuable discussions about fluid mechanics and surface-tension-driven corrugation of viscous materials.

REFERENCES

[1] D. J. Lougnot, in 'Radiation Curing in Polymer Science and Technology', Elsevier Appl. Sci., London, 1993, Chapt. 3.
[2] P. Hariharan, *Opt. Eng.* **1980**, *19*, 636; B. M. Monroe, *J. Imag. Sci.* **1991**, *35*, 25; R. T. Ingwald, M. Troll, *Opt. Eng.* **1989**, *28*, 586; Y. B. Boiko, V. S. Solovjev, S. Calixto, D. J. Lougnot, *Appl. Opt.* **1993**, *28*, 3904.
[3] A. Reiser, in 'Photoreactive Polymers', Wiley Interscience, New York, 1990, Chapt. 6.
[4] L. Landau, E. Lifschitz, 'Fluid Mechanics', MIR, Moscow, 1971, Chapt. 7.
[5] C. Croutxé-Barghorn, O. Soppera, D. J. Lougnot, *Appl. Surf. Sci.* **2000**, *168*, 89; C. Croutxé-Barghorn, D. J. Lougnot, *Pure Appl. Opt.* **1996**, *35*, 208.
[6] J. P. Fouassier, E. Chesneau, *Makromol. Chem.* **1991**, *192*, 245.
[7] D. J. Lougnot, in 'Techniques d'Utilisation des Photons', DOPEE, Paris, 1992, Chapt. 5.
[8] P. M. Costich, H. W. Osterhoudt, *J. Appl. Polym. Sci.* **1974**, *18*, 831.
[9] S. Wu, 'Surface and Interfacial Tensions of Polymers, Oligomers, Plasticizers, and Organic Pigments', in 'Polymer Handbook', Eds. J. Branrupt and E. H. Immergut, Wiley Interscience, New York, 1989, 3rd edn., p. VI/411.
[10] N. Mukolobwiez, Ph. D. Thesis, Saclay (France), 1998; R. A. L. Jones, R. W. Richards, 'Polymer at Surfaces and Interfaces', Cambridge Univ. Press, Cambridge, 1999; M. Hamdorf, D. Johannsmann, *J. Chem. Phys.* **2000**, *112*, 4262.
[11] J. Crank, 'The Mathematics of Diffusion', Oxford Univ. Press, London, 1956.
[12] R. B. Bird, W. E. Stewart, E. N. Lightfoot, 'Transport Phenomena', J. Wiley & Sons, New York, 1960.
[13] L. Nikolova, T. Todorov, *Opt. Acta* **1977**, *24*, 1179; T. Todorov, L. Nikolova, N. Tomova, *Appl. Opt.* **1984**, *23*, 4309.

Received June 15, 2001